https://doi.org/10.1007/s41230-019-9039-0

Prediction of mushy zone permeability of Al-4.5wt%Cu alloy during solidification by phase field model and CFD simulation

Long-fei Li[1], *Rui-jie Zhang[1], Shi-jie Hu[1], Dan Zhang[1], Shi-di Yang[2], Chang-sheng Wang[3], and Hai-tao Jiang[1]

1. University of Science and Technology Beijing, Beijing 100083, China

2. Sanying Precision Instruments Company Limited, Tianjin 300399, China

3. University of Shanghai for Science and Technology, Shanghai 200093, China

Abstract: Liquid permeability of the mushy zone is important for porosity formation during the solidification process. In order to investigate the permeability of the mushy zone, an integrated model was developed by combining the phase field model and computational fluid dynamics (CFD) model. The three-dimensional multigrain dendrite morphology was obtained by using the phase field model. Subsequently, the computer-aided design (CAD) geometry and mesh were generated based on calculated dendrite morphologies. Finally, the permeability of the dendritic mushy zone was obtained by solving the Navier-Stokes and continuity equations in ANSYS Fluent software. As an example, the dendritic mushy zone permeability of Al-4.5wt%Cu alloy and its relationship with the solid fractions were studied in detail. The predicted permeability data can be input to the solidification model on a greater length scale for macro segregation and porosity simulations.

Key words: phase field model; mushy zone; computational fluid dynamics; permeability; solidification

CLC numbers: TG146.21/TP391.9 **Document code:** A **Article ID:** 1672-6421(2019)05-313-06

Casting is a manufacturing process in which the liquid phase could transform to the solid phase. The solid fraction (f_s) is usually considered as a smoothly changing parameter from liquid to solid in macro scale. A solidifying casting can be divided into three different zones during solidification according to the solid fractions inside each zone, i.e. the liquid zone (f_s=0), the solid zone (f_s=1) and the mushy zone ($0<f_s<1$). The size of the mushy zone is several to tens of centimeters depending on the temperature gradient and the alloy compositions. This is schematically depicted in Fig. 1.

During solidification, the dendritic mushy zone can be considered as a permeable medium for liquid flow. The permeability is defined as a quantitative parameter to show how difficult it is for the liquid to pass through the mushy zone. Several research works [1-4] have demonstrated the influence of mushy zone permeability on solute segregation, porosity, and hot tearing formations. Additionally, permeability is a key parameter

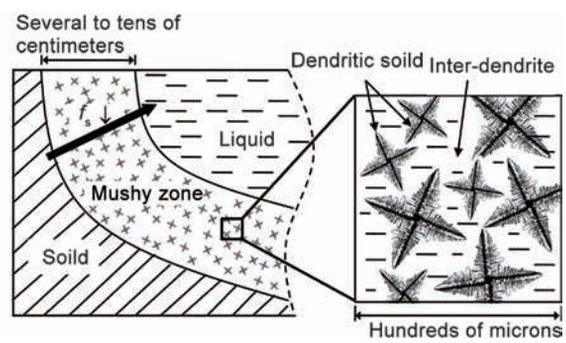

Fig. 1: Schematic diagram of mushy zone during solidification

constituting the Darcy term in a volume-averaged solidification model [5–8]. It describes the hydrodynamic drag in the momentum balance equation [9], which can be written as:

$$\frac{\partial(\tilde{\rho}\,\tilde{v})}{\partial t}+\nabla\cdot(\tilde{\rho}\,\tilde{v}\cdot\tilde{v})=\nabla\cdot(\mu_E\nabla\tilde{v})-\nabla\tilde{p}+\frac{\mu_E\tilde{v}}{K} \quad (1)$$

where $\tilde{\rho}$ is the liquid density, $\tilde{v}$ is the liquid-flow velocity vector, $\tilde{p}$ is the pressure. The wave-like notation over the variables represents the corresponding volume-averaged values. μ_E is the equivalent viscosity of the mixture. The value of permeability K must be predetermined to perform macro-scale simulations using

***Rui-jie Zhang**

Male, born in 1977, Associate Professor, His researches focus on the multi-scale modeling for solidification and solid state phase transformation.

E-mail: zrj@ustb.edu.cn

Received: 2019-03-20; Accepted: 2019-06-10

continuum solidification models. It is worth noting here that the permeability is a local physical parameter, its value greatly depends on the solid fraction at the corresponding location.

Since the permeability of the mushy zone is so important for the solidification process, a lot of researchers set up experiments to measure its value during the solidification process. It was firstly measured with forcing liquid lead throughout the solidifying Al-4.5wt%Cu alloy [10]. Additionally, investigations have previously been performed to obtain permeability values for different alloys, such as Al-Cu [11–17], Al-Si [18-21], and Pb-Sn [22-23]. However, it is difficult to measure liquid flow in the mushy zone, which had been discussed by Nielsen [24].

A number of physical models have previously been developed to investigate the mush-zone permeability. The first model describes the real dendrite morphology by a simplified geometric figure, such as spherical shape [18, 24, 25], cylinder [20] or cross mark [26-27]. In the second method, the real dendrite morphology was re-constructed by computed tomography [12, 28] or synchrotron X-ray tomography [29-30]. In the third method, a simulated dendritic solidification microstructure was adopted to re-construct the dendrite skeletons. The simulation can be executed by a phase field model [31-32] or a cellular automation model [20, 33].

Among the above-described physical models, the phase field model employs a continuously varying parameter Φ to characterize the solid-liquid phase interface. Accordingly, the complex interface pattern can be explicitly expressed using this powerful tool [34-38]. Besides microstructure evolutions, liquid flows can also be considered in the phase field model by coupling the Navier-Stokes and continuity equations into phase field equations [12]. Given that it is time consuming to perform three dimensional (3-D) phase field simulations, several acceleration techniques, such as parallel computation [39], graphical processing unit (GPU) [40], Fourier-spectral algorithms [34], and adaptive grid algorithms [41], have been employed. Nonetheless, the computational cost is still high when flow equations are fully coupled into 3D phase field models. Ludwig [31] and Böttger [32] performed computational fluid dynamics (CFD) calculations based on the dendrite morphology predicted using 3D phase field simulations. However, they considered only a single columnar dendrite.

In this work, the liquid permeability through the dendritic mushy zone with multiple equiaxed grains was studied. The CFD simulations were performed based on the predicted dendrite morphology generated by 3D phase field models. The proposed technique can be considered effective with regard to high geometric accuracy and computing efficiency. Permeability data obtained using the proposed technique could be used as input to macro-scale continuum solidification models. This will also be an important bridging method between different length scales when doing the multi-scale modeling, such as Integrated Computational Materials Engineering (ICME).

1 Mathematical model

1.1 3D dendrite simulation by phase field model

Different phases and orientations of polycrystalline systems should be accurately described during the solidification process, and this requires development of a multi phase field model, the evolution of which can be mathematically expressed as: [42–45]

$$\frac{\partial\varphi_\alpha}{\partial t}=\Sigma_\beta M_{\alpha\beta}\{\sigma_{\alpha\beta}[\varphi_\alpha\nabla^2\varphi_\beta-\varphi_\beta\nabla^2\varphi_\alpha+\frac{\pi^2}{\eta^2}(\varphi_\alpha-\varphi_\beta)]+\frac{\pi}{\eta}\sqrt{\varphi_\alpha\varphi_\beta}\,\Delta G_{\alpha\beta}^{CH}\} \quad (2)$$

where $M_{\alpha\beta}$ is the rate of interface migration; $\sigma_{\alpha\beta}$ is the interfacial energy; σ_α and σ_β are the phase field parameters; η is the interface width; and $\Delta G_{\alpha\beta}^{CH}$ is the chemical driving force, which can be expressed as follows:

$$\Delta G_{\alpha\beta}^{CH}=-f_\alpha(c_\alpha)+f_\beta(c_\beta)+\mu(c_\alpha-c_\beta) \quad (3)$$

where μ is the solute chemical potential. It can be expressed as follows [46-47]:

$$\mu=(\partial f_\alpha)/(\partial c_\alpha)=(\partial f_\beta)/(\partial c_\beta) \quad (4)$$

The local composition can be expressed as

$$c=\sum_{\alpha=1}^{N}\varphi_\alpha c_\alpha \quad (5)$$

where N is the total number of phases in the system.

It was reported that the inter-dendritic flow velocity driven by natural convection has the order of 10^{-6}–10^{-7} m·s^{-1}. Convection has little influence on dendritic growth when coupling with such slow fluid flows. Consequently, in this work, dendritic evolution was considered to occur under non-convective operating conditions. The governing equation for composition evolution can be expressed as

$$\frac{\partial c}{\partial t}=\nabla\Sigma_{\alpha=1}^{N}\varphi_\alpha D_\alpha\nabla c_\alpha \quad (6)$$

where D_α is the diffusion coefficient for phase α.

Simulated dendrite morphologies of the Al-4.5wt.%Cu alloy when f_s = 0.6 are depicted in Fig. 2 (a). The simulation domain comprised 300×300×300 grid points. The size of each element could be expressed as Δx = 2 μm, the interface width η=3.5 Δx. Corresponding simulation parameter values are listed in Table 1. Periodic boundary conditions were applied to the simulation domain.

1.2 Geometry re-construction and mesh generation for inter-dendrite liquid

To study the permeability of dendritic mushy zone via CFD simulations, CAD geometry files should first be generated based on the predicted dendrite morphology. This can be accomplished by exporting phase field results to a series of 2D image slices. For example, Fig. 2 (b) denotes the cross-sectional image of the phase field parameter for the case where in y = 300 μm. Since there exist 300×300×300 grid points within the computational domain, 300 such slices can be obtained, and the area of each slice is 600×600 μm^2. Providing these images as input to the commercial software AVZIO, the 3D geometry file and corresponding mesh for finite element analysis can be obtained. This process of inter-dendrite-liquid reconstruction is depicted in Fig. 3. In order to show the morphology of dendrite and inter-dendrite liquid more

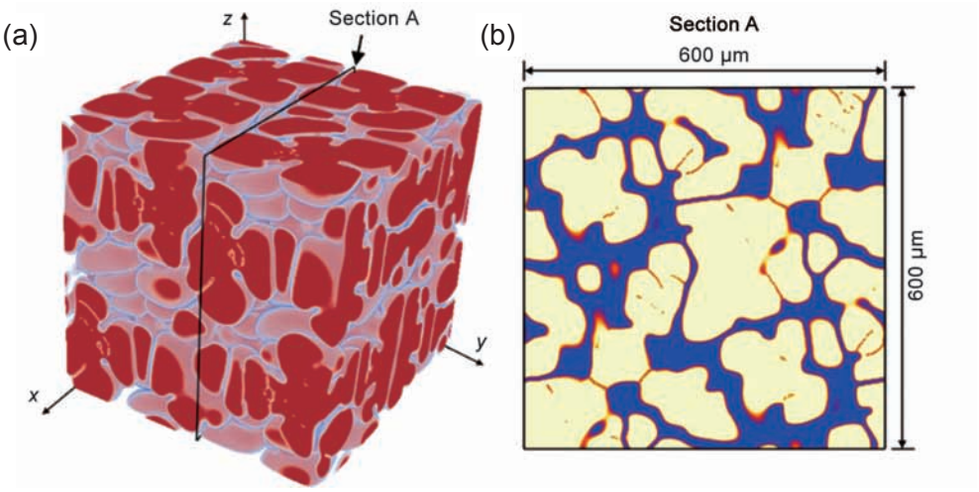

Fig. 2: Simulated dendritic solid skeleton by phase field model: (a) 3D morphology of dendrites; (b) One cross-sectional slice

Table 1: Simulation parameters used in this work

Parameters	Values
Coefficient of diffusion in liquid	2×10^{-8} $m^2\cdot s^{-1}$
Coefficient of diffusion in solid	1×10^{-12} $m^2\cdot s^{-1}$
Interfacial energy	0.1 $J\cdot m^{-2}$
Alloy concentration	Al-4.5 wt.% Cu
Interface-migration rate	4×10^{-10} $m^4\cdot J^{-1}\cdot s^{-1}$
Grid size	2×10^{-6} m

clearly, the complete dendrite morphology was reconstructed at different solid fractions, which can be seen in Fig. 4. It can be seen that the dendrite morphology and their evolutions can be well described by phase field models.

It is worth noting here that CFD simulations, in this case, can be performed using coarser meshes. From Fig. 2, it can be seen that there are 2.7×10^7 meshes for the phase field simulations. But for the CFD simulations, only 4×10^6 meshes are needed based on the same dendrite morphology, which can greatly reduce the computation time for solving the flow equations.

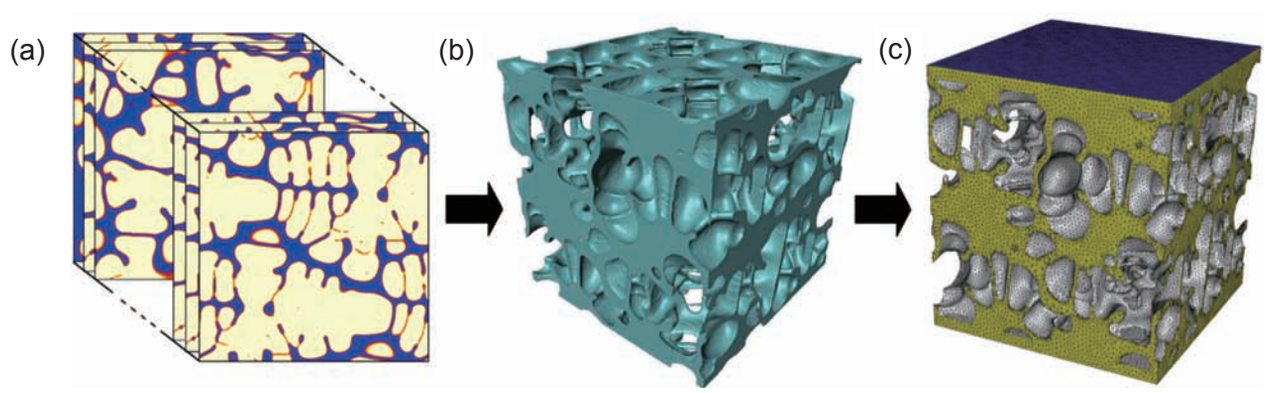

Fig. 3: Geometry reconstruction process for CFD simulations: (a) slices serial; (b) CAD geometry file; (c) meshes

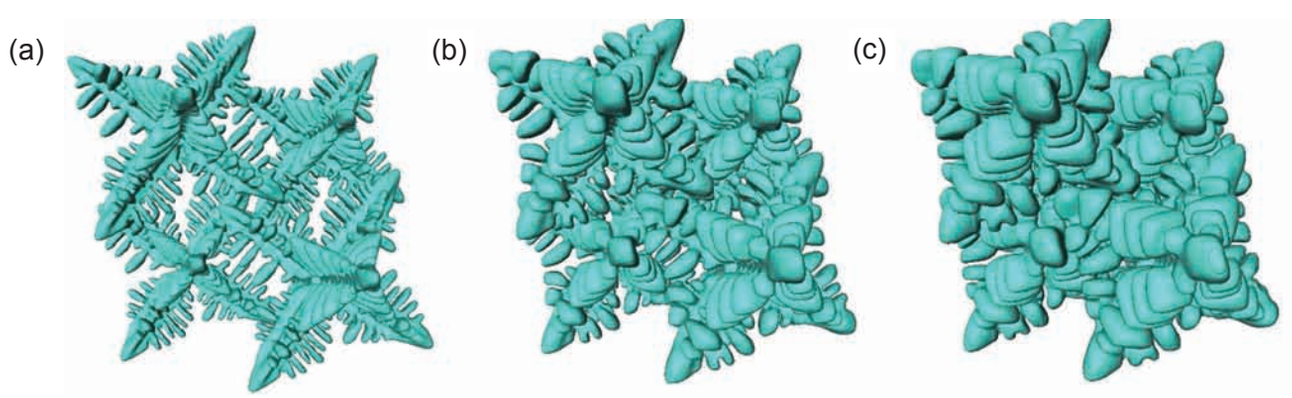

Fig. 4: Morphology of dendritic solid and their evolution in mush zone: (a) f_s = 0.1; (b) f_s = 0.3; (c) f_s= 0.6

1.3 CFD simulation of inter-dendrite flows

The Navier–Stokes and continuity equations over a smaller length scale, as described below, can be adopted to calculate permeability values concerning the dendritic mushy zone at different solid-fraction values.

$$\rho\left(\frac{\partial v}{\partial t}+v\cdot\nabla v\right)+\nabla p-\mu\nabla^2 v=0 \quad (7)$$

$$\nabla\cdot v=0 \quad (8)$$

where ρ is the density, v is the velocity vector, p is the pressure and μ is the liquid viscosity. It should be noted here that the parameters in Eq. (7) and Eq. (8) are all for the pure liquid phase.

In this work, values of the liquid density and viscosity were set as 1.26×10^3 kg·m^{-3} and 1.2×10^{-3} kg·m^{-1}·s^{-1}, respectively. The flow equations were solved using the commercial CFD software ANSYS Fluent. Boundary velocities during these simulations were set to a very small value (on the order of 10^{-7} m·s^{-1}). This is because the velocity of the inter-dendritic liquid driven by solidification shrinkage was rather small. No-slip conditions were applied at the inner walls of the computational domain to represent the solid-liquid interface. A laminar flow can be assumed in the simulation since the velocity is very small.

The pressure distribution predicted via CFD simulations performed with f_s = 0.6 is depicted in Fig. 5. Other simulations with different solid fractions were also performed in accordance with the methodology developed in this work.

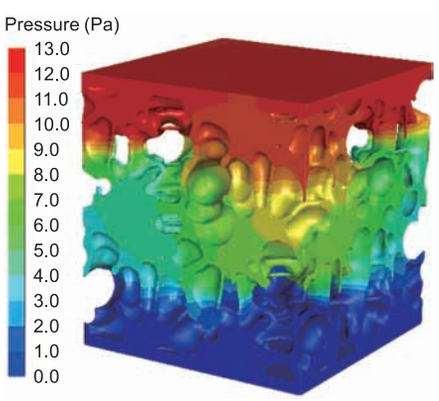

Fig. 5: Calculated pressure distribution within mush zone (f_s = 0.6)

2 Predicted permeability results of dendritic mushy zone

Based on results obtained from CFD simulations performed using different values of solid fractions, as described in Section 1.3, the permeability of the dendritic mushy zone can be expressed as

$$K=\mu vL/\Delta p \quad (9)$$

where K is the permeability; μ is the fluid viscosity; L is sample length; v is the fluid velocity at the inlet boundary; and Δp is the pressure drop between the inlet and outlet.

Figure 6 shows the predicted permeability as a function of f_s. The published experimental permeability data were also listed in Fig.6. It can be seen that the experimental results scattered too much at a fixed solid fraction. The predicted K-f_s curve was among those experimental data. As observed, the predicted value of permeability changes from $10^{-9.8}$ to $10^{-12.5}$ m^2 when f_s increases from 0.3 to 0.9. Additionally, differences can be observed between predicted values and experimental results owing to the following probable factors [15, 24]: (i) difference between wetting properties of the solid and flux metal (eutectic alloy, liquid lead, etc.); (ii) oxidation layer between the testing sample and flux metal. The authors intend to investigate these factors in greater detail in future studies.

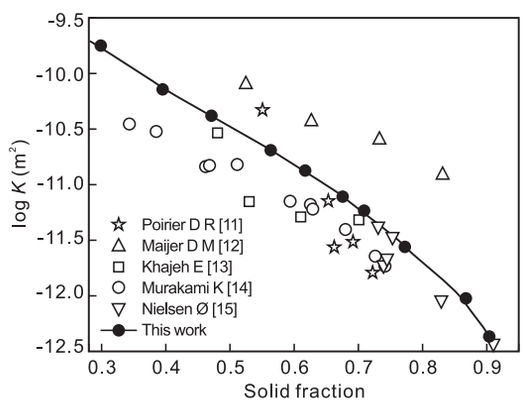

Fig. 6: Predicted values of mush-zone permeability as functions of f_s

In this work, predicted values of mush-zone permeability were also compared against those obtained using the Carman-Kozeny model, which is often used to describe the permeability of porous media [12,15]. The associated Carman–Kozeny equation can be expressed as:

$$KS_V^2=\frac{1}{k_c}\frac{(1-f_s)^2}{f_s^2} \quad (10)$$

where K is the permeability; S_v is the specific surface area of solid-liquid interface; and k_c is the Carman-Kozeny coefficient. During actual solidification processes, the value of S_v is usually obtained by quenching samples from the semi-solid state and subsequently performing quantitative metallographic analysis. However, using the model proposed in this work, values of parameters f_s, S_v, and K can all be obtained simultaneously. Predicted values of S_v as functions of f_s are depicted in Fig. 7. The published experimental data of S_v are also listed in Fig. 7.

For simplicity, the value of the Carman-Kozeny coefficient k_c in Eq. (10) was considered as the constant, which is a rather rough assumption. The said value has been assumed equal to 5 during the solidification process by several researchers [19, 48], albeit some studies have also suggested that the value of k_c cannot be considered as the constant during the entire solidification process [9, 12, 26, 49].

Using predicted values of f_s, S_v, and K obtained in this work, the value of k_c and its relationship with f_s can be deduced, as depicted in Fig. 8. As can be observed, the value of k_c greatly

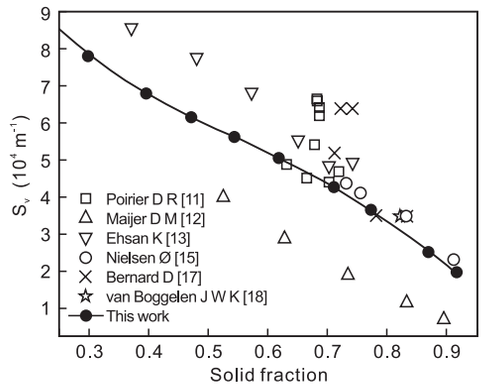

Fig. 7: Predicted values of S_v as functions of f_s

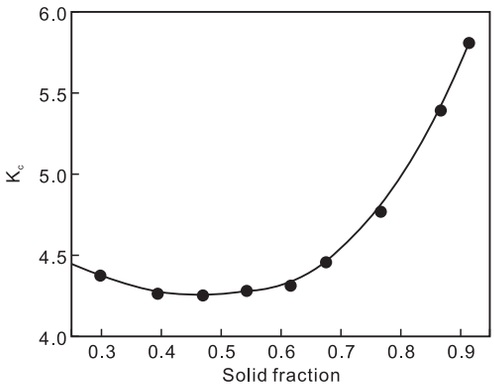

Fig. 8: Predicted values of Carman–Kozeny coefficient during solidification

changes during the entire solidification process. It approximately equaled to 4.5 when f_s< 0.7. This was followed by an exponential increase in the final solidification stage, where its value equaled to 5 or even more, corresponding to f_s>0.8. This may be attributed to the increased formation of closed-liquid regions during the final solidification stage. These areas could not play any roles for the liquid to go through the whole mushy zone.

3 Conclusions

In order to study the liquid permeability of the mushy zone, an integrated model was developed in this work by combining the phase field model and CFD model. Using the proposed technique, the equiaxed dendritic mush-zone permeability of Al-4.5wt.%Cu alloy has been investigated in detail. As observed, values of the permeability lie in the range of $10^{-9.8}$–$10^{-12.5}$ m^2 as corresponding values of the solid fraction change from 0.3 and 0.9. Moreover, the value of the Carman-Kozeny coefficient k_c was confirmed to equal approximately 4.5 at low solid fraction values (f_s<0.7). With increase in solid-fraction values (f_s>0.8), however, the value of k_c was observed to increase to 5.5 or even higher. These predicted permeability data can be used in the solidification model at a greater length scale for the macro segregation and porosity simulations.The integrated model developed in this work represents an important bridging method between different length scales when performing multiscale modeling in such applications as Integrated Computational Materials Engineering (ICME).

References

[1] Rappaz M, Drezet J M, Gremaud M. A new hot-tearing criterion. Metallurgical & Materials Transactions A, 1999, 30(2): 449–455.
[2] Sung P, Poirier D R, Felicelli S. Continuum model for predicting microporosity in steel castings. Modelling and Simulation in Materials Science and Engineering, 2002, 10(5): 551.
[3] Meidani H, Desbiolles J-L, Jacot A, et al. Three-dimensional phase-field simulation of micropore formation during solidification: Morphological analysis and pinching effect. Acta Materialia, 2012, 60(6–7): 2518–2527.
[4] Liu M, Wang K, Xia D, et al. Phase field simulation of Al-Si binary dendritic growth and micro-segregation patterns under convection. Journal of Alloys and Compounds, 2014, 589: 431–435.
[5] Pequet C, Rappaz M, Gremaud M. Modeling of microporosity, macroporosity, and pipe-shrinkage formation during the solidification of alloys using a mushy-zone refinement method: applications to aluminum alloys. Metallurgical and Materials Transactions A, 2002, 33(7): 2095–2106.
[6] Liu J, Kou S. Effect of diffusion on susceptibility to cracking during solidification. Acta Materialia, 2015, 100: 359–368.
[7] Stefanescu D M. Computer simulation of shrinkage related defects in metal castings – a review. International Journal of Cast Metals Research, 2005, 18(3): 129–143.
[8] Lee P, Chirazi A, See D. Modeling microporosity in aluminum–silicon alloys: a review. Journal of Light Metals, 2001, 1(1): 15–30.
[9] Liu J, Sano Y, Nakayama A. A simple mathematical model for determining the equivalent permeability of fractured porous media. International communications in heat and mass transfer, 2009, 36(3): 220–224.
[10] Piwonka T S, Flemings M C. Pore formation in solidification. Transactions of the Metallurgical Society of AIME, 1966, 236(8): 1157-1165.
[11] Poirier D R, Ganesan S. Permeabilities for flow of interdendritic liquid in equiaxial structures. Materials Science and Engineering: A, 1992, 157(1): 113–123.
[12] Khajeh E, Maijer D M. Permeability of dual structured hypoeutectic aluminum alloys. Acta Materialia, 2011, 59(11): 4511–4524.
[13] Khajeh E, Maijer D M. Permeability evolution during equiaxed dendritic solidification of Al-4.5 wt% Cu. Modelling and Simulation in Materials Science and Engineering, 2012, 20(3): 035004.
[14] Murakami K, Shiraishi A, Okamoto T. Fluid flow in interdendritic space in cubic alloys. Acta Metallurgica, 1984, 32(9): 1423–1428.
[15] Nielsen Ø, Arnberg S L, Mo A, et al. Experimental determination of mushy zone permeability in aluminum-copper alloys with equiaxed microstructures. Metallurgical and Materials Transactions A, 1999, 30(9): 2455–2462.
[16] Duncan A, Han Q, Viswanathan S. Measurement of liquid permeability in the mushy zones of aluminum-copper alloys. Metallurgical and Materials Transactions B, 1999, 30(4): 745–750.
[17] Bernard D, Nielsen Ø, Salvo L, et al. Permeability assessment by 3D interdendritic flow simulations on microtomography mappings of Al-Cu alloys. Materials Science and Engineering: A, 2005, 392(1-2): 112–120.
[18] van Boggelen J W K, Eskin D G, Katgerman L. Permeability of the mushy zone in aluminum alloys: Evaluation of different approaches. Edited by Paul N. Crepeau, Light Metals 2003, TMS, Warrendale, PA, 2003: 759–768.
[19] Han Q, Viswanathan S, Duncan A. Permeability measurements of the flow of interdendritic liquid in equiaxed aluminum-silicon alloys. Metallurgical and Materials Transactions B, 2003, 34(1): 25–28.
[20] Mirbagheri S, Chirazi A. Simulation of interdendritic liquid permeability for low and high solid fractions during the solidification of mushy alloys. Materials Science and Engineering: A, 2006, 427(1-2): 51–59.

[21] Zhao Z, Qi T, Hu P, et al. Alignment and permeability of Al-7Si alloy directional solidification with the application of a pulsed magnetic field. Materials and Manufacturing Processes, 2012, 27(5): 561–566.
[22] Poirier D R. Permeability for flow of interdendritic liquid in columnar-dendritic alloys. Metallurgical Transactions B, 1987, 18(1): 245–255.
[23] Khajeh E, Mirbagheri S, Davami P. Modeling of permeability with the aid of 3D interdendritic flow simulation for equiaxed dendritic structures. Materials Science and Engineering: A, 2008, 475(1-2): 355–364.
[24] Nielsen Ø, Arnberg L. Experimental difficulties associated with permeability measurements in aluminum alloys. Metallurgical and Materials Transactions A, 2000, 31(12): 3149–3153.
[25] Mirbagheri S. Modeling of the equiaxed dendrite coarsening based on the interdendritic liquid permeability during alloy solidification. Metallurgical and Materials Transactions B, 2008, 39(3): 469–483.
[26] Bhat M, Poirier D R, Heinrich J. Permeability for cross flow through columnar-dendritic alloys. Metallurgical and Materials Transactions B, 1995, 26(5): 1049–1056.
[27] Santos R, Melo M d L N M. Permeability of interdendritic channels. Materials Science and Engineering: A, 2005, 391(1-2): 151–158.
[28] Khajeh E, Maijer D M. Physical and numerical characterization of the near-eutectic permeability of aluminum–copper alloys. Acta Materialia, 2010, 58(19): 6334–6344.
[29] Liotti E, Lui A, Kumar S, et al. The spatial and temporal distribution of dendrite fragmentation in solidifying Al-Cu alloys under different conditions. Acta Materialia, 2016, 121: 384–395.
[30] Puncreobutr C, Phillion A, Fife J, et al. Coupling in situ synchrotron X-ray tomographic microscopy and numerical simulation to quantify the influence of intermetallic formation on permeability in aluminium–silicon–copper alloys. Acta Materialia, 2014, 64: 316–325.
[31] Ludwig A, Kharicha A, Hölzl C, et al. 3D Lattice Boltzmann flow simulations through dendritic mushy zones. Engineering Analysis with Boundary Elements, 2014, 45: 29–35.
[32] Böttger B, Haberstroh C, Giesselmann N. Cross-permeability of the semisolid region in directional solidification: a combined phase-field and lattice-Boltzmann simulation approach. JOM, 2016, 68(1): 27–36.
[33] Brown S, Spittle J, Jarvis D, et al. Numerical determination of liquid flow permeabilities for equiaxed dendritic structures. Acta Materialia, 2002, 50(6): 1559–1569.
[34] Chen L Q. Phase field models for microstructure evolution. Annual Review of Materials Research, 2002, 32(1): 113–140.
[35] Steinbach I. Phase field models in materials science. Modelling and Simulation in Materials Science and Engineering, 2009, 17(7): 073001.
[36] Qin R, Bhadeshia H. Phase field method. Materials Science and Technology, 2010, 26(7): 803–811.
[37] Wang Y, Li J. Phase field modeling of defects and deformation. Acta Materialia, 2010, 58(4): 1212–1235.
[38] Fabrizio M, Giorgi C, Morro A. A thermodynamic approach to non-isothermal phase-field evolution in continuum physics. Physica D: Nonlinear Phenomena, 2006, 214(2): 144–156.
[39] Culler D, Karp R, Patterson D, et al. LogP: Towards a realistic model of parallel computation. ACM Sigplan Notices, ACM, 1993: 1–12.
[40] Takaki T, Sakane S, Ohno M, et al. Primary arm array during directional solidification of a single-crystal binary alloy: large-scale phase-field study. Acta Materialia, 2016, 118: 230–243.
[41] Gao Y, Rong H, Huang J Z. Adaptive grid job scheduling with genetic algorithms. Future Generation Computer Systems, 2005, 21(1): 151–161.
[42] Apel M, Benke S, Steinbach I. Virtual dilatometer curves and effective Young's modulus of a 3D multiphase structure calculated by the phase-field method. Computational Materials Science, 2009, 45(3): 589–592.
[43] Steinbach I, Apel M. Multi phase field model for solid state transformation with elastic strain. Physica D: Nonlinear Phenomena, 2006, 217(2): 153–160.
[44] Steinbach I. Phase field model for microstructure evolution at the mesoscopic scale. Annual Review of Materials Research, 2013, 43: 89–107.
[45] Böttger B, Eiken J, Steinbach I. Phase field simulation of equiaxed solidification in technical alloys. Acta Materialia, 2006, 54(10): 2697–2704.
[46] Kim S G, Kim W T, Suzuki T. Phase field model for binary alloys. Physical Review E, 1999, 60(6): 7186.
[47] Schmitz G, Böttger B, Apel M. On the role of solidification modelling in Integrated Computational Materials Engineering "ICME". IOP Conference Series: Materials Science and Engineering, IOP Publishing, 2016, p. 012041.
[48] Sun Z, Logé R E, Bernacki M. 3D finite element model of semi-solid permeability in an equiaxed granular structure. Computational Materials Science, 2010, 49(1): 158–170.
[49] Khajeh E, Maijer D. Numerical determination of permeability of Al-Cu alloys using 3D geometry from X-ray microtomography. Materials Science and Technology, 2010, 26(12): 1469–1476.

This work was financially supported by the National Key Research and Development Program of China (No.2016YFB0700503), National Natural Science Foundation of China (No.51701013), Funds from Beijing Laboratory of Metallic Materials and Processing for Modern Transportation.